Sensors & Diagnostics

COMMUNICATION

View Article Online
View Journal | View Issue

Cite this: *Sens. Diagn.*, 2024, **3**, 1461

Received 8th March 2024,
Accepted 22nd July 2024

DOI: 10.1039/d4sd00076e

rsc.li/sensors

A handheld laser-cut device for the size-controlled assembly and electrical characterisation of lipid bilayers†

Ji Huang,[ab] Yuval Elani [cd] and Mark S. Friddin [*ad]

We report the rapid fabrication of a handheld laser cut platform that can support the assembly, functionalisation, size-control and electrical characterisation of lipid bilayers. We achieve this by building a modular DIY platform that can support the lowering of a Ag/AgCl electrode through a phase transfer column consisting of an upper oil phase containing lipids, and a lower aqueous phase containing buffer.

Synthetic phospholipid bilayers have been used for decades as *in vitro* models for studying the biophysical properties of lipid membranes, membrane proteins, and for screening for protein-drug interactions.[1] In recent years, the field has experienced a renaissance through the introduction of new methods that can generate and functionalise artificial lipid bilayers on miniature Lab-on-a-Chip devices.[2–4] This has led to new applications in fields such as artificial cell engineering,[5] drug delivery,[6] soft robotics,[7] and biosensing,[8,9] with new areas such as vesicle computing & robotics emerging as assemblies become more elaborate in terms of their functionality.[10,11]

Compared to conventional methods for characterising native cellular membranes (*e.g.* Patch-clamp), the major advantage of working with artificial lipid bilayers is that biomimetic cell membranes can be rapidly formed without the direct need for biological cells, while also allowing for systematic investigations by affording users complete control over bilayer composition. The drawbacks are the varied bilayer lifetimes, the requirement for users to supply and incorporate membrane proteins, and in many cases, the need for specialised pieces of equipment, tools and/or facilities for microengineering.[12,13] For example, the classic approach of forming aperture-suspended lipid bilayers (also known as bilayer/black lipid membranes, BLMs) traditionally relies on users engineering or procuring small apertures in polymer substrates (typically <200 μm in diameter); the generation of unilamellar vesicles often requires dispersions to be electroformed, or extruded through a nanoporous membrane;[14] while microfluidic platforms, which can be used to engineer a variety of different lipid bilayer assemblies,[5] are typically manufactured in cleanrooms using soft lithography.[13]

In addition to the requirements for bilayer formation, the specifications of setups can be further complicated depending on the readout strategy employed by investigators. It is in this context that fluorescence microscopy is a popular option, as it only demands optical accessibility to the bilayer and the absence of any background signal or significant autofluorescence, whereas electrical measurements using a variant of the Patch-clamp method can offer direct characterisation of the bilayer to pA sensitivity but requires Ag/AgCl electrodes to be positioned either side of the bilayer, and for the entire setup to be placed inside of a Faraday cage enclosure to shield from electrical noise. This can be quite straightforward for aperture suspended lipid bilayers as electrodes can be submerged in relatively large buffer-filled chambers, but is often more challenging when working with microdroplets that are a <2 mm in diameter, as is required for the electrical characterisation of droplet interface bilayers (DIBs).[15] This configuration is attractive as it offers the ability to compartmentalise cargos in small (nL – pL) volumes and form bilayers by placing single, or successive, lipid-monolayer coated water droplets into contact. However, this approach not only calls for visualisation of the microdroplets, but can require hydrogel-tipping (to promote adhesion to the microdroplets) and the precise positioning of the electrodes in the *X*, *Y* and *Z* dimensions.[15,16] These factors motivate

[a] *Dyson School of Design Engineering, Imperial College London, Exhibition Road, South Kensington, SW7 2AZ, London, UK. E-mail: m.friddin@imperial.ac.uk*
[b] *Centre for Neurotechnology, Imperial College London, SW7 2AZ, London, UK*
[c] *Department of Chemical Engineering, Imperial College London, Exhibition Road, South Kensington, SW7 2AZ, London, UK*
[d] *fabriCELL, Imperial College London and Kings College London, London, UK*
† Electronic supplementary information (ESI) available. See DOI: https://doi.org/10.1039/d4sd00076e

efforts to design simple and low-cost platforms for the formation and electrical characterisation of lipid bilayers that users can quickly and easily manufacture, assemble, and operate themselves. This has been reported recently for the droplet contact method, which is essentially a DIB separated by an aperture, where the entire platform (including apertures) was 3D printed and fitted with Ag/AgCl electrodes for readout.[17] Herein, we present an alternative approach to device fabrication, lipid bilayer formation and electrical interrogation by reporting a handheld platform that can be rapidly manufactured using a standard CO_2 laser cutter (Fig. 1). We demonstrate how 10 modular parts can be manufactured from flat sheets of PMMA and assembled in less than 30 minutes into a functional instrument that fits on a standard 75 × 26 mm microscope slide. Using our platform, we show that lipid bilayers can be rapidly formed on our device by passing an unencapsulated Ag/AgCl electrode through a phase transfer column, that these bilayers can functionalised with the constitutively active membrane pore alpha-hemolysin (α-HL), blocked with the reversible blocker TRIMEB (heptakis(2,3,6-tri-*O*-methyl)-β-cyclodextrin), and be assembled to controllable sizes. Our approach allows for the simple and rapid assembly of lipid bilayers, while the scale and form factor of our platform also makes it fully portable, lending well to performing measurements in a wide variety of settings.

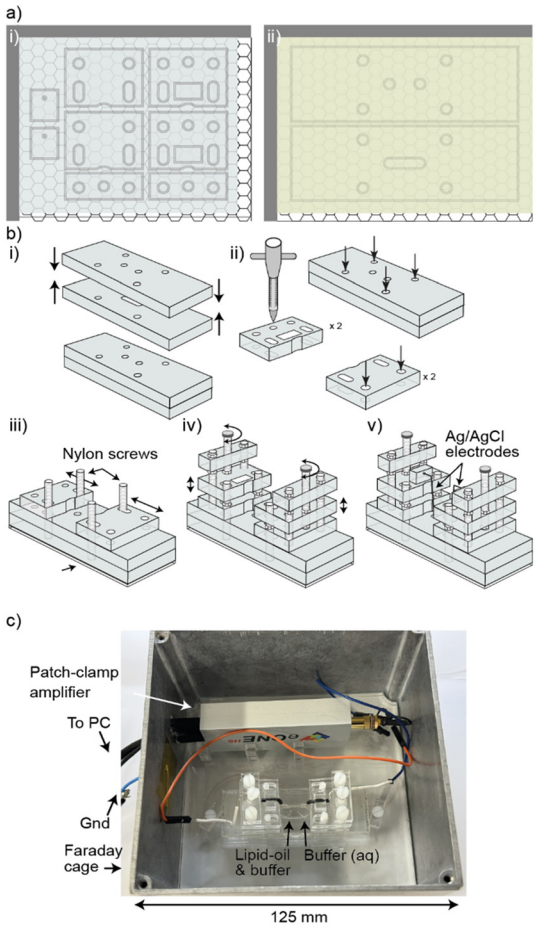

Fig. 1 Rapid manufacturing and assembly of our CO_2 laser cut device. a) Laser cutting. Parts designed in CAD were laser cut from 5 mm thick sheets of i) plain PMMA or ii) PMMA prepared with double-sided adhesive. b) Assembly. i) The phase transfer column was assembled *via* the double-sided adhesive and ii) relevant holes (indicated by the arrows) were threaded using an M2 hand tap. iii) A glass slide was fixed to the base of the phase transfer column using double sided adhesive and nylon screws (with their heads removed) were inserted into the threaded holes to support the installation of a tray for moving the electrodes in the forward and backward directions. iv) Nylon screws (with their heads removed) were inserted into the threaded holes of the tray to support a second tray (with a cavity for the electrode holder) for moving the electrode up and down. A top bracket was installed to secure the assembly and to support an M2 screw that was threaded through the second tray. After the addition of nylon nuts in the indicated positions, the platform could be raised or lowered by turning the indicated screw clockwise our counterclockwise. v) Electrode holders housing Ag/AgCl electrodes were inserted into the cavities by push fit. c) A photograph of our setup placed inside our Faraday cage.

All parts used in our setup were designed in CAD (SolidWorks, see ESI† Fig. S1 for dimensions) and laser cut (Universal Laser Systems, USA) using default settings from either one plain sheet of 5 mm thick PMMA (Weatherall, UK), or a 5 mm thick sheet of PMMA prepared with double-sided adhesive (3 M, USA) as shown in Fig. 1a) i) and ii). The parts containing the double-sided adhesive were bonded together to create the phase transfer column (as shown in part i) of Fig. 1b)), which consisted of a part containing a 16 mm long × 6 mm wide channel, and a part containing two holes 6 mm in diameter – this was designed to contain the oil within the phase transfer column and exclude it from the well containing the ground electrode (depicted by the rectangular piece shown in the centre of illustrations in Fig. 2). The next stage in manufacturing the setup was to manually thread the relevant holes (as indicated by the arrows in part ii) if Fig. 1b)) using an M2 hand tap (RS Components, UK). The process of assembling of our setup is depicted in parts iii) – v) of Fig. 1b). First, the remaining strip of double-sided adhesive on the bottom of the phase transfer column was used to bond a glass microscope slide, and M2 Nylon screws (with their heads removed) were installed into the tapped holes of the base to support the installation of stages for providing movement in the forward and backward directions (Fig. 1b), part iii)). Next, M2 Nylon screws (also with their heads removed) were inserted into the tapped holes of both stages to secure the installation of a second stage which provided movement upwards and downwards direction. This movement was achieved using an M2 Nylon screw that was threaded through a hole in the back of the stage and secured *via* a M2 Nylon nut. The addition of a bracket at the top of the assembly supported the positioning of this screw and prevented sideways movement of the second stage, meaning that the second stage housing our Ag/AgCl electrodes could be raised and lowered by turning the screw clockwise or counterclockwise (Fig. 1b), part iv). The final stage of assembling our device was the insertion of electrode

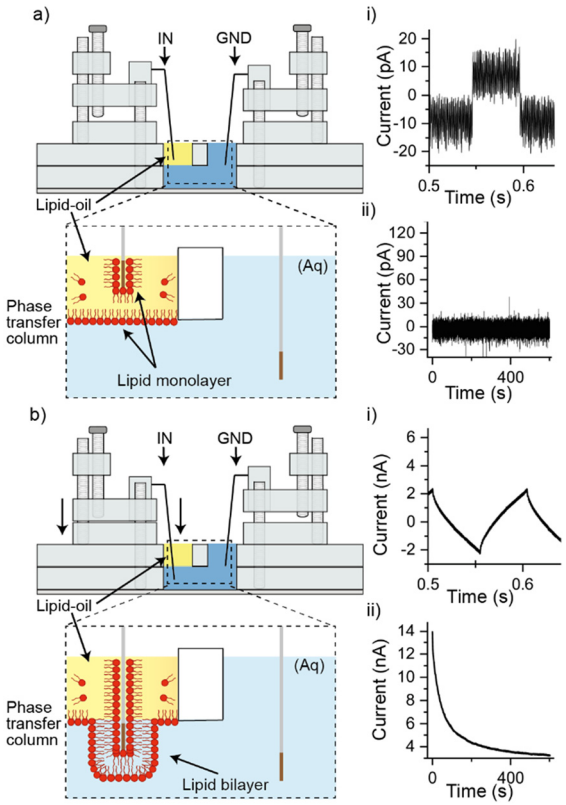

Fig. 2 Device operation (illustrations show cross-sectional view). a) The Ag/AgCl electrode connected to the input of the amplifier was lowered into the upper section of the phase transfer column containing lipid–oil. The insert shows a magnified illustration of the phase transfer column (not to scale). i) Capacitance measurements in this configuration show a background capacitance of ~8 pA while bilayer current measurements at +100 mV in ii) show a baseline around 0 pA. b) Illustration showing the measuring electrode after being lowered down the phase transfer column and through the oil : water interface after a 10-minute incubation, alongside an insert showing a magnified perspective (not to scale). i) Capacitance measurements in this configuration either show saturation (indicating the absence of a lipid bilayer), or a bilayer capacitance (as shown). ii) Bilayer current measurements at +100 mV either showed saturation in this configuration, or bilayer currents of several nA. Bilayer current traces were captured using the 20 nA range on the amplifier, a sampling rate of 20 kHz and a final bandwidth of SR/20. They were also digitally filtered using a low-pass Gaussian filter with a cut-off frequency of 1 kHz.

holders, 8.5 × 10 mm blocks of PMMA with 0.63 mm holes for securing Ag/AgCl electrodes in heat shrink, which were designed to push-fit into a cavity on the stage (Fig. 1b, part v). The setup was then transferred to a customised 125 × 125 × 75 mm aluminium box (RS Components, UK), which was used as a Faraday cage, and the Ag/AgCl electrodes were connected to a miniature (74 × 30 × 15 mm) eOne amplifier (Elements SRL, IT), which was fixed in position using laser cut clamps. A photograph of our entire setup is shown in Fig. 1c). To operate our platform (Fig. 2), the 16 × 6 mm wide channel at the base of our phase-transfer column was filled with 580 μl of 150 mM KCl, 10 mM HEPES, pH 7.4 and the well closest to the Ag/AgCl electrode connected to the input of the amplifier was filled with 150 μl of 5 mg ml^{-1} 1,2-dioleoyl-*sn-glycero*-3-phosphocholine (DOPC) (Avanti Polar Lipids, USA) in hexadecane (Sigma, UK) (see ESI† for details of preparation). The addition of the lipid–oil to this well displaced the underlying buffer solution allowing it to partially fill the opposite well for the Ag/AgCl electrode connected to ground. Ag/AgCl electrodes were electroplated in pairs from 0.5 mm thick silver (Goodfellow, UK). The amplifier was configured to allow lipid bilayers to be probed in two ways. Capacitance tests were performed by applying a symmetric triangle wave function as the membrane potential. Where dV/dT = 1 V s^{-1} the bilayer current can be interpreted as the bilayer capacitance through the relation $I = (dV/dT) \times C$. This test is indicative of the presence of a lipid bilayer, and by assuming a specific bilayer capacitance of 0.5 μF cm^{-2}, allows for its size to be estimated.[18] In addition to the bilayer capacitance, the bilayer current was also measured directly when applying a +100 mV voltage clamp.

In the absence of membrane proteins, this measurement can provide insight into the integrity of the bilayer and is expected to yield a bilayer current close to 0 pA in the presence of a well-formed, intact lipid bilayer.[19]

When performing experiments, the Ag/AgCl electrode connected to ground was lowered into the aqueous chamber, while the recording electrode was lowered into the lipid–oil for 10 minutes, as illustrated in Fig. 2a). In this configuration a negligible background capacitance of ~8 pA was observed as shown in part i) of Fig. 2a) (n = 3) and the bilayer current showed a baseline fixed at around 0 pA with no leakage currents (n = 3), as depicted in part ii) of Fig. 2a). This outcome is expected in the absence of a conduction pathway between the two electrodes, while the background capacitance can be attributed to a small feedback capacitor in the amplifier as reported previously.[20] When the Ag/AgCl electrode positioned in the oil phase was lowered down the phase transfer column, through the interface, and into the aqueous phase (as illustrated in Fig. 2b), we observed either a capacitance as shown in Fig. 2b) part i), or the saturation of our instrument (indicating the absence of a lipid bilayer). The average capacitance measured was 641 pF ± 127 pF, rising to an average of 1.73 nF ± 0.57 nF after 15 minutes (n = 5), suggesting the presence of a lipid bilayer with an average bilayer area of 12.82 μm^2 ± 2.54 μm^2 rising to 34.6 μm^2 ± 11.4 μm^2. This inference was supported by our bilayer current measurements as shown in part ii) of Fig. 2b), which reveal leakage currents at around 4 nA following an initial stabilisation phase (n = 5). While this trend is similar to what is often seen in measurements of DIBs, the leakage current is approximately an order of magnitude higher than what would normally be expected.[20] The presence of leakage currents on this scale are indicative of significant bilayer defects,[19] most likely owing to the size of the bilayer and the method of bilayer assembly. Leakage currents of this nature would also be expected to give rise to the distortion in the capacitance traces shown in part i) of Fig. 1c). To test the

reliability of our approach, the above steps were repeated 30 times, with a bilayer capacitance similar to that shown in part i) of Fig. 1c) observed on 15 occasions and the saturation of our instrument (indicating the absence of a lipid bilayer) on the remaining 15 attempts. While the reliability of bilayer formation is known to vary between approaches, the 50% success rate of our approach is broadly in-line with what has been reported previously for DIBs assembled from DOPC in hexadecane.[21] Our method can also be rapidly reset by simply withdrawing the electrode back to the oil phase, lending well to automation. To investigate the conformity of the bilayer to our Ag/AgCl electrode we tipped the measuring electrode with agar and observed an increase in the initial bilayer capacitance to an average of 15.36 nF ± 2.21 nF (n = 3), corresponding to an average bilayer area of 307.2 μm^2 ± 44.2 μm^2 (see ESI† Fig. S2), suggesting a close link between the electrode diameter and the bilayer size.

To verify the presence of a lipid bilayer, alpha haemolysin (αHL) (Sigma, UK) was premixed to the desired concentration in buffer and added as part of the 580 µl volume dispensed into the lower chamber of our setup. αHL is a 33.2 kDa water soluble heptameric nanopore that is known to self-insert into lipid bilayers and remain constitutively open, giving rise to discrete 'step-like' increases in the bilayer current when individual pores become active.[22] Although this single-pore behaviour is not expected to be observed in our setup due to the size and low resistance of our lipid bilayers, successful incorporation of αHL should render the bilayer more permeable and result in an increase in the bilayer current.[23] Consistent with previous reports,[22] an initial concentration of 50 ng μl^{-1} was selected for experiments however these conditions repeatedly resulted in the saturation of the amplifier (indicating the absence of a lipid bilayer) when bilayer formation was attempted (n = 5). In contrast, a capacitance was observed when the αHL concentration was reduced to 5 ng μl^{-1}. A representative measurement of the bilayer current at +100 mV (n = 3) is shown in Fig. 3a), which shows an initial reduction of the bilayer current to <2 nA followed by a steady increase to over 8 nA over the course of the 10 min experiments (see ESI† Fig. S3 for details of additional repeats). This increase in the bilayer current is not only consistent with the successful insertion of αHL, but is also different to the controls shown in Fig. 2, thereby indicating the presence of a lipid bilayer. We infer that the initial concentration of 50 ng μl^{-1} prevented the assembly of our lipid bilayers due to the scale of insertion events. To support this inference further, the reversible blocker TRIMEB (heptakis(2,3,6-tri-*O*-methyl)-*b*-cyclodextrin) (Sigma, UK) was dissolved in buffer and premixed with αHL to yield a final concentration of 10 mM. This volume was dispensed into the lower chamber of our setup as described and the Ag/AgCl electrode was passed through the interface after a 10-minute incubation in the oil phase. A representative measurement of the bilayer current at +100 mV (n = 3) is shown in Fig. 3b), which shows the same initial decrease in

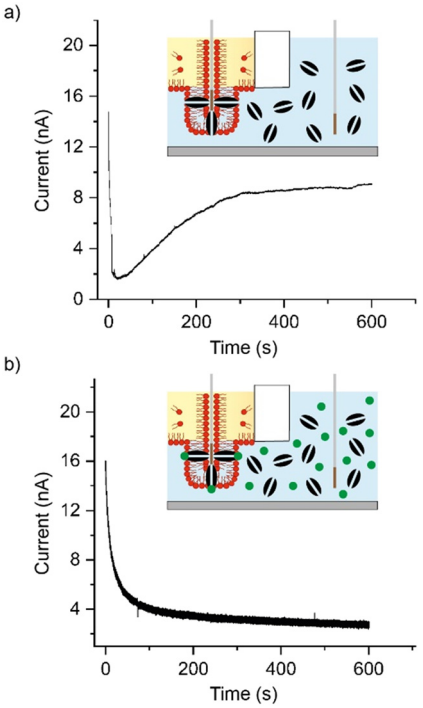

Fig. 3 Bilayer functionalisation with nanopores and blockers. a) Representative trace showing the bilayer current becoming more permeable to ion flow in the presence of αHL. b) Trace showing the reversal of additional bilayer current when in the presence of TRIMEB (green circles). Bilayer current traces were captured using the 20 nA range on the amplifier, a sampling rate of 20 kHz and a final bandwidth of SR/20. They were also digitally filtered using a low-pass Gaussian filter with a cut-off frequency of 1 kHz.

the bilayer current to *ca.* 4 nA where the baseline remains for the duration of our 10-minute experiments (see ESI† Fig. S4 for details of additional repeats). Our results are similar to what was observed in our controls (Fig. 2) and show a complete reversal of the elevated bilayer current observed in the presence of αHL alone, indicating that TRIMEB is actively blocking the nanopore.[23] This confirms that lipid bilayers can be successfully assembled using our minimal, rapid prototyped setup. As indicated in the illustrations accompanying Fig. 2) and 3), we attribute the mechanism of bilayer formation in our platform to the assembly of a lipid monolayer on the surface of our Ag/AgCl electrode and at the oil–water interface, with a lipid bilayer being extruded as the two monolayers come into contact as the electrode is lowered through the interface and into the aqueous phase. Our ability to capture electrical measurements of the bilayer confirms that water must be present on both sides, which likely arises from diffusion of the aqueous phase through bilayer defects (appearing in our recordings as leakage currents). Our proposal of bilayer formation is consistent with previous studies that report the formation of membranes at these interfaces,[24–26] and in principle should permit some size-control of the lipid bilayer formed by regulating the final position of the Ag/AgCl electrode after it passes through the interface.

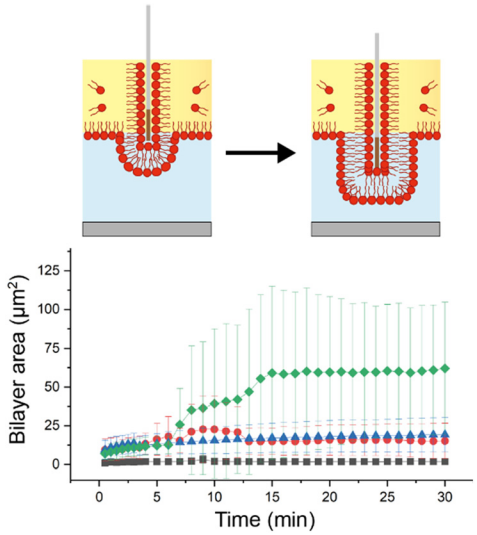

Fig. 4 Control of bilayer area by lowering the measuring electrode to different positions though the oil–water interface. Data points correspond to translation distances of 1.5 mm (n = 3, squares), 2.0 mm (n = 6, circles), 2.5 mm (n = 5, triangles) and 3.0 mm (n = 4, diamonds). The data shows that the area of the bilayer increases with translation distance. Illustrations do not show the ground electrode.

To investigate this property in our setup, we configured the starting position of the Ag/AgCl electrode such that a fully retracted screw corresponded to a location that resided within the oil phase. After a 10-minute incubation in this position, the electrode was lowered by turning the nylon screw by 3, 4, 5 or 6 complete turns (corresponding to a travel distance of 1.5 mm,

2 mm, 2.5 mm and 3 mm given the 0.5 mm pitch of the thread) and the bilayer capacitance was measured at 30 s intervals for 30 min. The average from a minimum of three repeats for each condition are plotted in Fig. 4, where the measured bilayer capacitance has been converted into bilayer area in μm^2. These measurements show that lipid bilayers with average areas ranging from *ca.* 1.8 μm^2 (3 turns, squares in Fig. 4) to *ca.* 62 μm^2 (6 turns, diamonds) can be successfully engineered using our device. The data also reveals some initial convergence between data points obtained from experiments where the electrode was lowered by 4 (circles), 5 (triangles) and 6 turns, however the average bilayer area appears to stabilise after *ca.* 6 min and plateau after 15 min, at which point the measurements appear in order of translation distance, where it remains for the duration of our experiments. While this data supports our hypothesis for the mechanism of bilayer formation, it is of note that there are varying degrees of experimental variation associated with our measurements. This is expected when working with stochastic systems such as lipid bilayers, particularly when they are large and when the oil–water interface is not directly regulated.[27] Further, the ability to precisely position the electrode using our rapid prototyped approach is likely to be another contributing factor that impacts our measurements. In addition to experimental variation, it is also noticeable that the values obtained for the average bilayer size are smaller and less distributed than expected when considering the Ag/AgCl electrode as a cylinder with a diameter of 0.5 mm. This could in-part be explained by the morphology of the lipid bilayer formed on the electrode surface and the presence of excess oil but may also be connected to the geometry of the electrode. To investigate this parameter we detached our measuring electrode from our setup and imaged it using brightfield microscopy (see ESI† Fig. S5). This revealed a chamfer at the electrode tip (most likely from the wire cutters used) which reduced its surface area and modified its shape, explaining the reduced size of the bilayers formed in our experiments.

Conclusions

In conclusion, we have shown the assembly, functionalisation, size-control and electrical characterisation of lipid bilayers using a handheld platform that can be rapidly and inexpensively engineered using a standard workshop CO_2 laser cutter. Our results highlight how investigators can harness the power of design and rapid prototyping to create bespoke miniature instruments that can be readily customised according to the needs of users. Moreover, by demonstrating that lipid bilayers formed using our approach can be sensitised to different chemical inputs, we show that meaningful data can be captured using our system despite the presence of leakage currents. These may be reduced in future iterations of our approach by introducing polymers or PEGylated lipids,[28] by reducing the size of the well and/or diameter of the electrodes. Developing a greater understanding of the interaction between the electrode and the lipids, as well as the kinetics of the oil–water interface will also likely also contribute to higher success rates of future iterations of the device. By inserting other membrane proteins (*e.g.* MscL or KcsA) it should also be possible to sensitise our platform to different chemical, mechanical and/or electrical inputs, particularly as these channels are known to give rise macroscopic currents when open-state.[29,30] This ability to engineer nanomaterials that can sense and respond to different stimuli using low cost and easy to manufacture platforms could have significant impact on the development of the next generation of deployable biosensors, especially if our approach can be multiplexed using a multi-well format. In addition, our approach to the flatpack assembly of instruments using laser cutting could have wider implications for the design engineering of devices for other applications in redistributed manufacturing, as well as for establishing digital manufacturing pipelines.

Data availability

The data supporting this article have been included as part of the ESI.†

Author contributions

MSF conceived the study and designed and built the setup. MSF and YE supervised JH who performed the experiments. MSF wrote the manuscript. MSF produced the figures/illustrations.

Conflicts of interest

There are no conflicts to declare.

Acknowledgements

This work was supported by an Imperial College Research Fellowship awarded to MSF.

Notes and references

1 M. Trojanowicz and A. Mulchandani, *Anal. Bioanal. Chem.*, 2004, **379**, 347–350.
2 P. S. Dittrich and A. Manz, *Nat. Rev. Drug Discovery*, 2006, **5**, 210–218.
3 M. Zagnoni, *Lab Chip*, 2012, **12**, 1026–1039.
4 M. R. R. De Planque, *Jpn. J. Appl. Phys.*, 2022, **61**, SC0804.
5 T. Trantidou, M. S. Friddin, A. Salehi-Reyhani, O. Ces and Y. Elani, *Lab Chip*, 2018, **18**, 2488–2509.
6 M. Maeki, N. Kimura, Y. Sato, H. Harashima and M. Tokeshi, *Adv. Drug Delivery Rev.*, 2018, **128**, 84–100.
7 J. Čejková, T. Banno, M. M. Hanczyc and F. Štěpánek, *Artif. Life*, 2017, **23**, 528–549.
8 F. Mazur, M. Bally, B. Städler and R. Chandrawati, *Adv. Colloid Interface Sci.*, 2017, **249**, 88–99.
9 T. Osaki and S. Takeuchi, *Anal. Chem.*, 2017, **89**, 216–231.
10 R. Kawano, *ChemPhysChem*, 2018, **19**, 359–366.
11 Z. Peng, S. Iwabuchi, K. Izumi, S. Takiguchi, M. Yamaji, S. Fujita, H. Suzuki, F. Kambara, G. Fukasawa, A. Cooney, L. Di Michele, Y. Elani, T. Matsuura and R. Kawano, *Lab Chip*, 2024, **24**, 996–1029.
12 S. Demarche, K. Sugihara, T. Zambelli, L. Tiefenauer and J. Vörös, *Analyst*, 2011, **136**, 1077–1089.
13 M. S. Friddin, Y. Elani, T. Trantidou and O. Ces, *Anal. Chem.*, 2019, **91**, 4921–4928.
14 T. Trantidou, M. Friddin, Y. Elani, N. J. Brooks, R. V. Law, J. M. Seddon and O. Ces, *ACS Nano*, 2017, **11**, 6549–6565.
15 H. Bayley, B. Cronin, A. Heron, M. A. Holden, W. L. Hwang, R. Syeda, J. Thompson and M. Wallace, *Mol. BioSyst.*, 2008, **4**, 1191–1208.
16 R. Syeda, M. A. Holden, W. L. Hwang and H. Bayley, *J. Am. Chem. Soc.*, 2008, **130**, 15543–15548.
17 K. Ogishi, T. Osaki, Y. Morimoto and S. Takeuchi, *Lab Chip*, 2022, **22**, 890–898.
18 S. Aghdaei, M. E. Sandison, M. Zagnoni, N. G. Green and H. Morgan, *Lab Chip*, 2008, **8**, 1617–1620.
19 M. S. Friddin, H. Morgan and M. R. R. de Planque, *Biomicrofluidics*, 2013, **7**, 014108.
20 M. S. Friddin, N. P. Smithers, M. Beaugrand, I. Marcotte, P. T. F. Williamson, H. Morgan and M. R. R. De Planque, *Analyst*, 2013, **138**, 7294–7298.
21 G. A. Venkatesan, J. Lee, A. B. Farimani, M. Heiranian, C. P. Collier, N. R. Aluru and S. A. Sarles, *Langmuir*, 2015, **31**, 12883–12893.
22 G. Villar, A. J. Heron and H. Bayley, *Nat. Nanotechnol.*, 2011, **6**(12), 803–808.
23 J. M. Thomas, M. S. Friddin, O. Ces and Y. Elani, *Chem. Commun.*, 2017, **53**, 12282–12285.
24 K. Karamdad, J. W. Hindley, G. Bolognesi, M. S. Friddin, R. V. Law, N. J. Brooks, O. Ces and Y. Elani, *Chem. Sci.*, 2018, **9**, 4851–4858.
25 C. G. Siontorou, G. P. Nikoleli, D. P. Nikolelis and S. K. Karapetis, *Membranes*, 2017, **7**(3), 38.
26 K. Shoji, R. Kawano and R. J. White, *Anal. Chem.*, 2020, **92**, 10856–10862.
27 S. A. Sarles and D. J. Leo, *Anal. Chem.*, 2010, **82**, 959–966.
28 M. J. Booth, V. R. Schild, A. D. Graham, S. N. Olof and H. Bayley, *Sci. Adv.*, 2016, **2**, e1600056.
29 R. Strutt, J. W. Hindley, J. Gregg, P. J. Booth, J. D. Harling, R. V. Law, M. S. Friddin and O. Ces, *Chem. Sci.*, 2021, **12**, 2138–2145.
30 S. Chakrapani, J. F. Cordero-Morales and E. Perozo, *J. Gen. Physiol.*, 2007, **130**, 465–478.